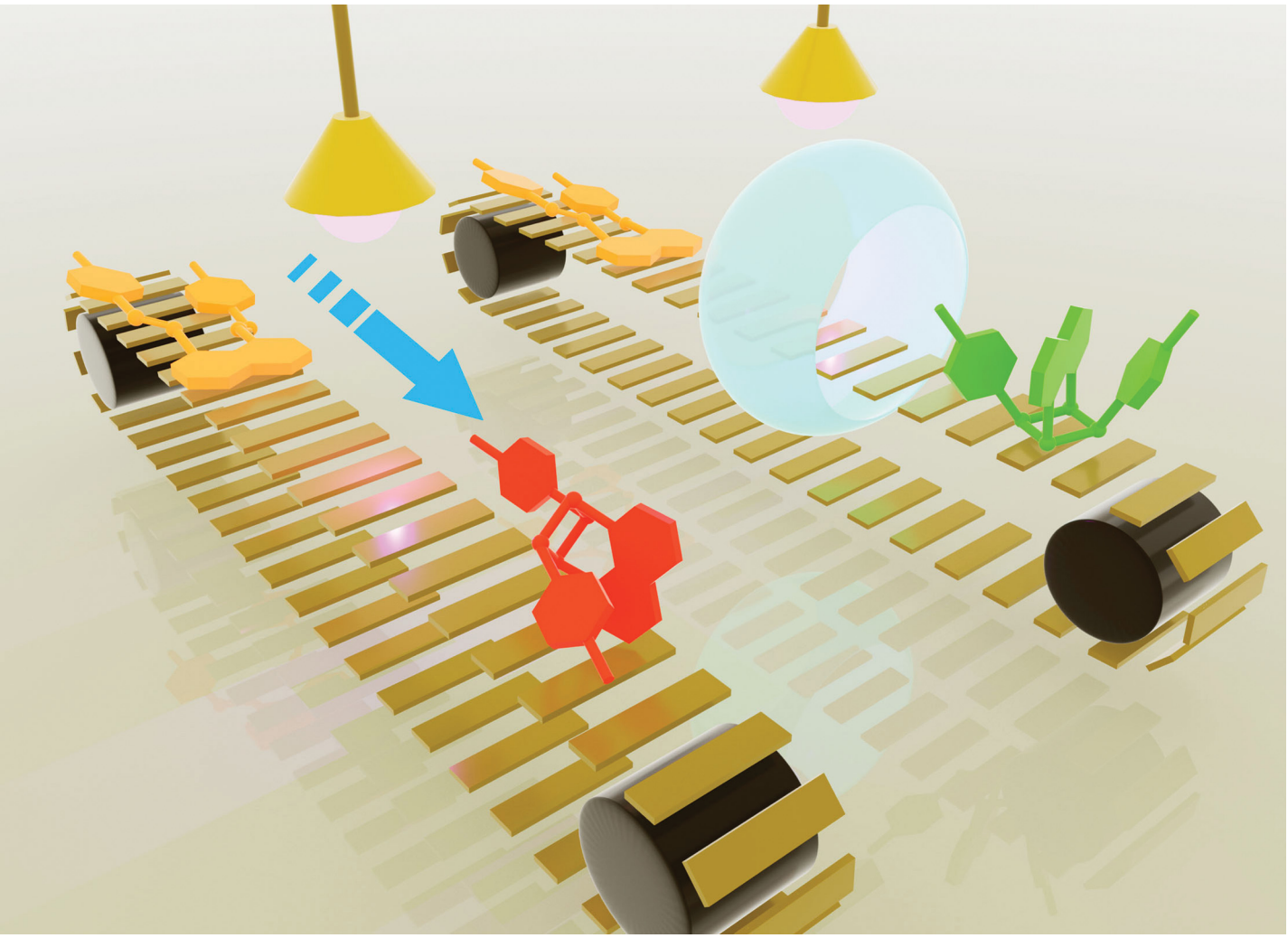

Showcasing research from Professor Stefan Bräse's laboratory, Institute of Organic Chemistry, Karlsruhe Institute of Technology (KIT), Karlsruhe, Germany.

Reversing the stereoselectivity of intramolecular [2+2] photocycloaddition utilizing cucurbit[8]uril as a molecular flask

Reactions can be tuned using the confined space of supramolecular hosts. In this work, we showcase the intrinsic role cucurbit[8]uril plays in modulating the outcome of an intramolecular [2+2] photocycloaddition.

As featured in:

See Frank Biedermann, Stefan Bräse *et al.*, *Chem. Commun.*, 2024, **60**, 3267.

ROYAL SOCIETY OF CHEMISTRY

rsc.li/chemcomm

Registered charity number: 207890

ChemComm

ROYAL SOCIETY OF CHEMISTRY

COMMUNICATION

View Article Online
View Journal | View Issue

Open Access Article. Published on 02 February 2024. Downloaded on 4/8/2024 12:59:06 PM.
This article is licensed under a Creative Commons Attribution 3.0 Unported Licence.

Check for updates

Cite this: *Chem. Commun.*, 2024, **60**, 3267

Received 27th November 2023,
Accepted 29th January 2024

DOI: 10.1039/d3cc05783f

rsc.li/chemcomm

Reversing the stereoselectivity of intramolecular [2+2] photocycloaddition utilizing cucurbit[8]uril as a molecular flask†

Xujun Qiu,[a] Jasmin Seibert,[a] Olaf Fuhr,[bc] Frank Biedermann *[b] and Stefan Bräse *[ad]

Macrocyclic hosts, such as cucurbit[8]uril (CB8), can significantly influence the outcomes of chemical reactions involving encapsulated reactive guests. In this study, we demonstrate that CB8 completely reverses the stereoselectivity of intramolecular [2+2] photo-cycloaddition reactions. Notably, it was also found that CB8 can trigger the unreactive diene to be reactive.

Cyclobutanes, with their inherently strained scaffolds, are pivotal in numerous natural products and biological systems.[1,2] The prevalent synthetic routes to cyclobutanes often employ inter/intramolecular [2+2] photo-cycloadditions using olefin precursors.[3] Moreover, intramolecular [2+2] cycloadditions are commonly used to synthesize bioactive natural products.[4] Yet, achieving precise control over the stereoselectivity of the photo [2+2] cycloaddition remains challenging.

Recent advancements in carrying out organic reactions within "molecular flasks",[5,6] specifically using supramolecular hosts, such as macrocycles,[7–9] cages[10–14] and capsules,[15–17] have paved the way for novel reaction pathways. The reactivity and selectivity of reagents is controlled by the microenvironment, *e.g.*, the confined space within the cavity of molecular flasks assists in preorganizing the substrates,[18,19] which modulates the reaction rates or steers reactions in directions distinct from those in bulk solutions.

Cucurbit[*n*]urils (CB*n*) are characterized by their symmetrical, rigid, and hydrophobic cavities that can host organic molecules.[20,21] Their nanocavities are excellent binders for hydrophobic molecules in aqueous environments, while the carbonyl-fringed portal regions provide an additional driving force for binding cationic guests. As a result, CB*n* have been employed as both reaction vessels and supramolecular catalysts[22,23] to control or accelerate the outcome of organic reactions such as 1,3-dipolar Huisgen cycloaddition,[24–26] Diels–Alder reaction, and photodimerization.[27–29]

In this study, we showcase how the outcome of intramolecular [2+2] photocycloaddition can be switched from an *anti*-head-to-tail to a *syn*-head-to-tail cycloaddition product using CB8 as a molecular flask. Furthermore, it was also found that CB8 can trigger the unreactive diene to be reactive, yielding a *syn*-head-to-head (1,2) product. As depicted in Scheme 1, diene **1** experiences intramolecular charge repulsion due to its two cationic methylpyridinium moieties. We started our investigation with the photolysis of **1** in water, using a standard photoreactor fitted with 14 UVA (365 nm) lamps. ^{1}H NMR spectra (Fig. S4, ESI†) were recorded at fixed time intervals to monitor the reaction path.

As irradiation progressed, the ^{1}H peaks from **1** gradually disappeared, while new signals corresponding to a single intramolecular cycloaddition product emerged. After approximately 18 minutes of UV exposure, no further significant changes were observed in the NMR spectra, indicating the completion of the photolysis. Structural assignment of the product peaks revealed that UV irradiation of **1** in water proceeds *via* photoisomerization and [2+2] cycloaddition, yielding an *anti*-head-to-tail (1,3) product where the charge repulsion between the pyridinium moieties is minimized (refer to Fig. S7–S15 in the ESI† for a detailed structural assignment of the reaction product.)

Intrigued by the potential impact of a confined environment on the photoreaction process, we explored whether the photoisomerization of molecule **1** could be inhibited within the cavity of a molecular host, and whether this altered the outcome of the [2+2] cycloaddition. We selected the water-soluble

[a] *Institute of Organic Chemistry (IOC), Karlsruhe Institute of Technology (KIT), Kaiserstraße 12, 76131 Karlsruhe, Germany. E-mail: braese@kit.edu*
[b] *Institute of Nanotechnology (INT), Karlsruhe Institute of Technology (KIT), Kaiserstraße 12, 76131 Karlsruhe, Germany. E-mail: frank.biedermann@kit.edu*
[c] *Karlsruhe Nano Micro Facility (KNMFi), Karlsruhe Institute of Technology (KIT), Kaiserstraße 12, 76131 Karlsruhe, Germany*
[d] *Institute of Biological and Chemical Systems-Functional Molecular Systems (IBCS-FMS), Karlsruhe Institute of Technology (KIT), Kaiserstraße 12, 76131 Karlsruhe, Germany*

† Electronic supplementary information (ESI) available. CCDC 2309696. For ESI and crystallographic data in CIF or other electronic format see DOI: **https://doi.org/10.1039/d3cc05783f**

Open Access Article. Published on 02 February 2024. Downloaded on 4/8/2024 12:59:06 PM.
This article is licensed under a Creative Commons Attribution 3.0 Unported Licence.

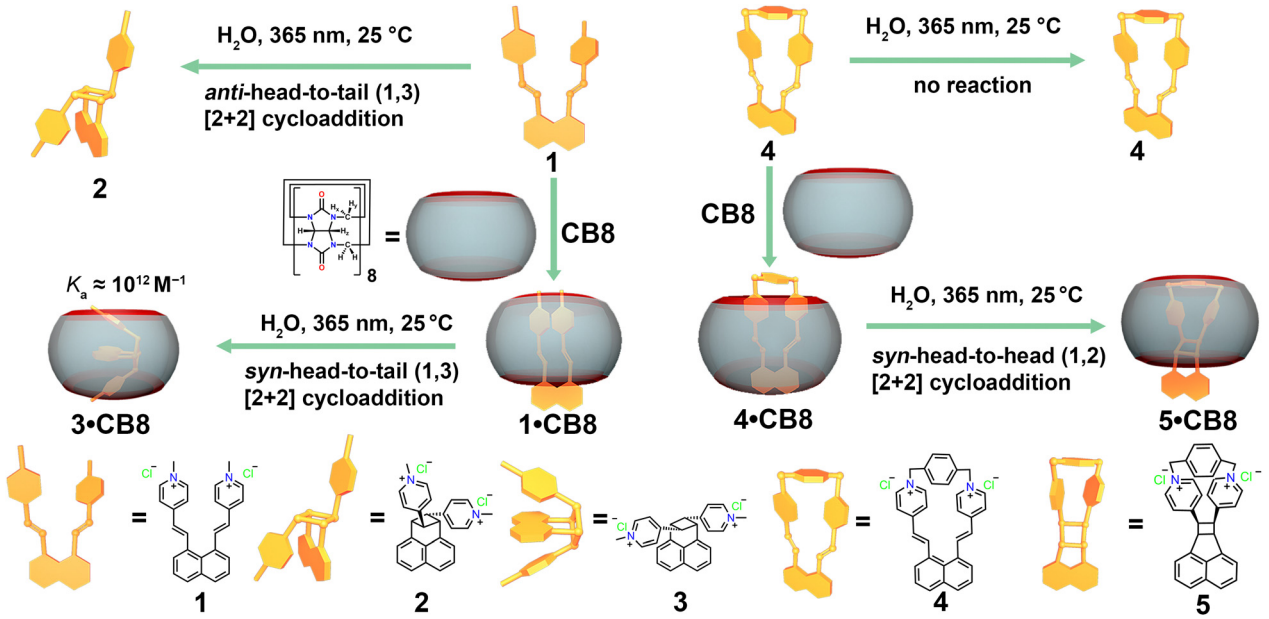

Scheme 1 Schematic illustration of modulating the photolysis reaction outcome of **1** utilizing cucurbit[8]uril as a molecular flask.

molecular host CB8 as our choice, given its spacious and hydrophobic cavity, which could accommodate both vinylpyridinium residues of **1** simultaneously. To test this binding hypothesis, we first examined the host–guest properties between **1** and CB8 using ^{1}H NMR. As depicted in Fig. 2a, when an aqueous solution of **1** and CB8 was mixed in a 1 : 1 ratio in D_2O, the NMR signals a–d, corresponding to the vinylpyridinium residues, showed significant upfield shifts, indicating that these are bound inside the shielding CB8 cavity. Conversely, the peaks corresponding to the naphthyl moieties (e–g) displayed slight downfield shifts, suggesting that these moieties are located outside or near the rim of the CB8 portal.[30] Notably, the signals H_x and H_y from CB8 split into four sets, reflecting the deformation of CB8 when molecule **1** is accommodated within its cavity. The formation of the 1 : 1 complex of **1**·CB8 was further confirmed by ESI-MS experiments (Fig. S16, ESI†), where a peak with a mass-to-charge ratio (m/z) of 846.2923 for $[\mathbf{1}\cdot\text{CB8-2Cl}]^{2+}$ was observed.

We further explored the binding affinity between **1** and CB8 through UV titration, gradually introducing CB8 into a solution of **1**. As depicted in Fig. 1b, the addition of CB8 led to a decrease in absorbance, with the two maximum absorbance peaks at 281 nm and 396 nm shifting to isosbestic points 293 nm and 421 nm, respectively. We plotted the changes in absorbance at 281 nm against the concentration of CB8, as shown in Fig. 1c. Least-square fitting of this data with a direct binding assay (DBA) model yielded a binding constant of $(2.53 \pm 0.11) \times 10^6$ M^{-1}, indicating a strong interaction between **1** and CB8.

Furthermore, we performed the photoreaction of **1** encapsulated in the CB8 cavity under the same photoreaction conditions as for **1** in water for comparison. Upon irradiation, the ^{1}H NMR signals were observed to be completely different from

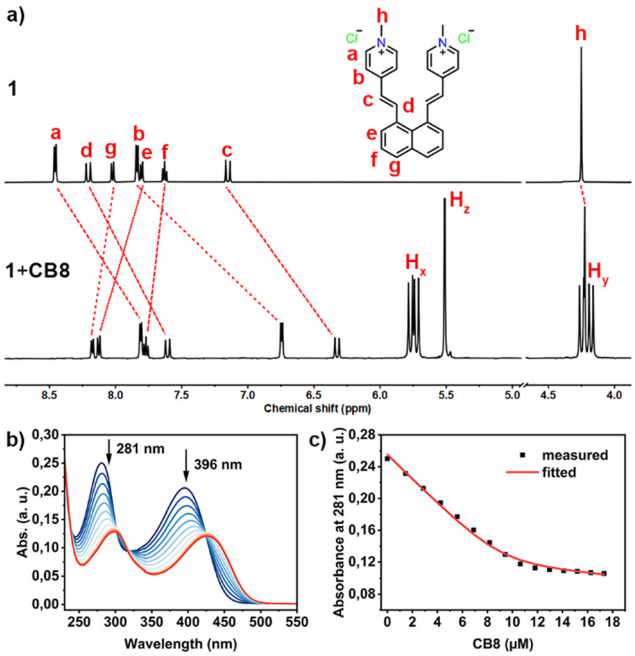

Fig. 1 (a) Partial ^{1}H NMR spectra of **1** (0.5 mM) and **1** + CB8 (1 : 1, 0.5 mM) in D_2O; (b) UV-vis titration spectra of **1** (**1** = 10 μM) upon addition of CB8 (CB8 = 0–17.3 μM) in an aqueous solution at 298 K; (c) least-square curve fitting of the UV absorbance changes at 281 nm against the concentration of CB8 for determining the binding constant between **1** and CB8.

the initial state, suggesting the formation of new species (Fig. S19, ESI†). After around 21 min, no more significant variation in the NMR suggests the end of the reaction.

A similar phenomenon in UV absorbance and fluorescence emission change was observed (Fig. S20 and S21, ESI†). As shown in Fig. 2b, the absorbance was observed to decrease

Open Access Article. Published on 02 February 2024. Downloaded on 4/8/2024 12:59:06 PM.
This article is licensed under a Creative Commons Attribution 3.0 Unported Licence.

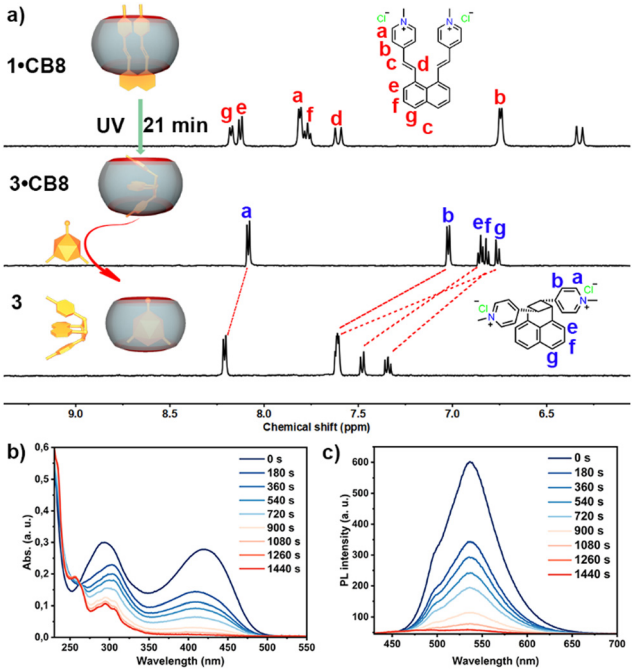

Fig. 2 (a) ^{1}H NMR spectra of **1**·CB8 (1 : 1, 0.5 mM), **3**·CB8 (1 : 1, 0.5 mM), and **3** (0.5 mM), in the aromatic region in D_2O; (b) UV-vis spectra of **1**·CB8 (1 : 1, 0.5 mM, diluted to 20 μM for UV-vis measurements) upon irradiation at 298 K; (c) emission spectra of **1**·CB8 (1 : 1, 0.5 mM, and diluted to 20 μM for UV-vis measurements) upon irradiation at 298 K (excited at 410 nm).

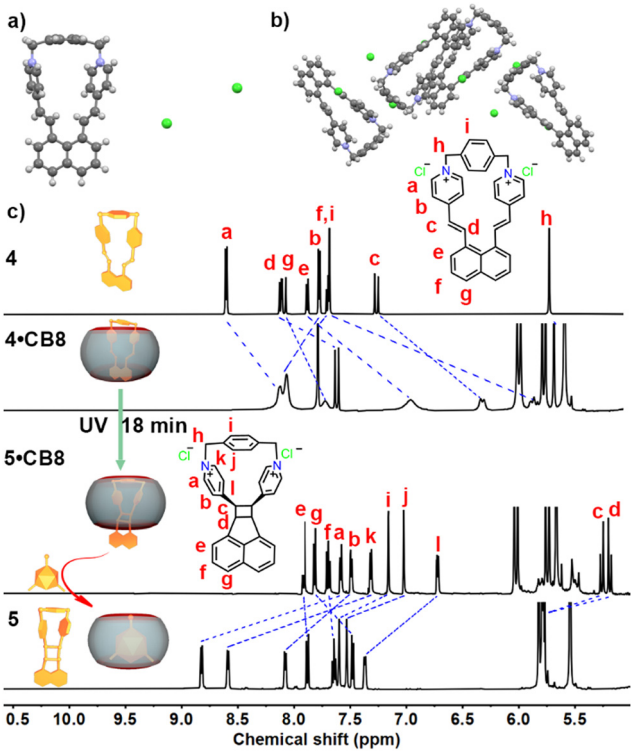

Fig. 3 (a) Molecular structure of **4** (front view, water molecules are omitted for clarity); (b) crystal packing of **4** (water molecules are omitted for clarity); (c) ^{1}H NMR spectra of **4**, **4**·CB8 (1 : 1, 0.5 mM), **5**·CB8 (1 : 1, 0.5 mM), and **5** (0.5 mM) in D_2O; for full spectra see Fig. S27, S31, S38 and S40 (ESI†).

dramatically within the first 3 min, in which the maximum absorption peak at 421 nm was eventually barely visible after being irradiated for 21 min. The fluorescence intensity was identical upon UV irradiation, which decreased rapidly to no emission at the end, Fig. 2c. The formation of [2+2] cycloaddition product **3** in the CB8 cavity was also evidenced by ESI-MS (Fig. S24, ESI†), in which a strong signal peak with a mass-to-charge ratio (*m/z*) of 846.2927 that corresponded to $[\mathbf{3}\cdot\mathrm{CB8}\text{-}2\mathrm{Cl}]^{2+}$ was observed, which suggested no mass change of **3** in the CB8 cavity compared to starting reagent **1**.

Upon addition of the strongly CB8-binding competitive guest, memantine hydrochloride, to the **3**·CB8 complex, unbound **3** was obtained, as shown in Fig. 2a (for full spectra see Fig. S25, ESI†). The symmetric signals in Fig. 2a (Fig. S25, ESI†) indicate a *syn*-head-to-tail (1,3) photo cycloaddition product **3**, which is different from the similar structure reported in the literature.[31] Notably, the binding constant of **3** between CB8 was determined to be $(2.04 \pm 0.29) \times 10^{12}$ M^{-1} using a competitive binding assay (CBA), where memantine was utilized as a competitive guest (Fig. S42, ESI†).[32] The dramatically increased binding constant of **3** compared with starting molecule **1** could result from the rigidified structure of **3** having a better complemental effect with the CB8 void. Further studies were conducted to understand the mechanistic pathway of the reaction. The rate of product formation was found to be significantly influenced by the concentration of CB8, suggesting a pivotal role of the macrocycle in the reaction kinetics. Control experiments, conducted in the absence of CB8 or in the presence of smaller macrocycle CB7 that cannot fully encapsulate **1** in its cavity due to sterical reasons, further corroborated its role in steering the reaction towards the *syn*-head-to-tail (1,3) cycloaddition product. In the meantime, controlled experiments in the dark under thermal conditions were performed for **1** and **1**·CB8, and no reaction traces were observed for both cases. To gain more insights into the stereo structures of the different possible products, we performed theoretical calculations and predicted the NMR composition (Table S1, ESI†), which further supported our conclusions.

We then wondered whether the photo cycloaddition process could still take place if two olefin branches were covalently locked. Therefore, molecule **4**, in which the pyridine moieties were bridged by 1,4-bis(bromomethyl)benzene, was designed, synthesized, and fully characterized (Fig. S27–S29, ESI†). As shown in Fig. 3a and b, the crystal structure suggests that molecule **4** bears a rigid structure and the olefin groups are separated distinctly. Thus, photolysis of molecule **4** in aqueous media results in no change. In the same fashion, we then studied the host–guest interaction between **4** and CB8. Indeed, molecule **4** can be encapsulated within the CB8 cavity, as indicated by the ESI-MS (Fig. S30, ESI†), and NMR spectra (Fig. S31, ESI†). The NMR spectra of **4** and **4**·CB8 suggest that CB8 selectively encapsulates a naphthyl moiety, while the bridged pyridinium locates at the carbonyl portal of the CB8, which is comparable to the literature.[33] The binding constant

Open Access Article. Published on 02 February 2024. Downloaded on 4/8/2024 12:59:06 PM.
This article is licensed under a Creative Commons Attribution 3.0 Unported Licence.

of **4** and CB8 was obtained using UV-vis titration, which was fitted as $(2.52 \pm 0.15) \times 10^6$ M^{-1} (Fig. S33, ESI†).

Surprisingly, upon the irradiation of **4**·CB8 under the same reaction conditions as photolysis of **1** and **1**·CB8, new species were observed in the NMR spectra (Fig. 3c and Fig. S34, ESI†). Absorption (Fig. S35, ESI†) and emission spectra (Fig. S36, ESI†) also revealed the occurrence of the photoreaction. The mass spectra (Fig. S37, ESI†) of the **5**·CB8 complex suggest no mass change of the photoreaction product. The NMR spectra (Fig. 3c and Fig. S38, ESI†) indicate that a dissymmetric product is formed, and the identical signal at 5.18–5.27 ppm suggests that the *syn*-head-to-head (1,2) cycloaddition product is generated, which is comparable to the similar structure.[31] To obtain unbound product **5** out of the CB8 cavity, memantine hydrochloride was introduced to the reaction mixture (Fig. 3c and Fig. S40, ESI†).

In conclusion, we presented a strategy to selectively tune the photoreaction pathway utilizing CB8 as a molecular flask. The photoreaction of molecule **1** in bulk water was assisted with the photoisomerization and [2+2] cycloaddition process, resulting in an *anti*-head-to-tail (1,3) photoproduct **2**. However, with the template from CB8, the photoreaction selectively formed *syn*-head-to-tail (1,3) cycloaddition product **3**. Notably, the binding constant between **3** and CB8 was estimated to be as high as $(2.04 \pm 0.29) \times 10^{12}$ M^{-1}. When molecule **4** was intramolecularly locked, photoreaction was prevented upon irradiation. On the contrary, when the photoreaction was performed inside the CB8 cavity, a *syn*-head-to-head (1,2) product was obtained.

The authors acknowledge the support of the China Scholarship Council (CSC grant: 202010190002) and the Deutsche Forschungsgemeinschaft (DFG) under Germany's Excellence Strategy-3DMM2O-EXC-2082/1-390761711. F. B. acknowledges the Deutsche Forschungsgemeinschaft (DFG grant BI-1805/2-1) for financial support.

Conflicts of interest

There are no conflicts to declare.

References

1 J. C. J. M. D. S. Menezes and M. F. Diederich, *Eur. J. Med. Chem.*, 2019, **182**, 111637.
2 T. Bach and J. P. Hehn, *Angew. Chem., Int. Ed.*, 2011, **50**, 1000–1045.
3 S. Poplata, A. Tröster, Y.-Q. Zou and T. Bach, *Chem. Rev.*, 2016, **116**, 9748–9815.
4 M. D. Kärkäs, J. A. Porco, Jr. and C. R. J. Stephenson, *Chem. Rev.*, 2016, **116**, 9683–9747.
5 M. Yoshizawa, J. K. Klosterman and M. Fujita, *Angew. Chem., Int. Ed.*, 2009, **48**, 3418–3438.
6 B. Breiner, J. K. Clegg and J. R. Nitschke, *Chem. Sci.*, 2011, **2**, 51–56.
7 P. Zhang, J. Meijide Suárez, T. Driant, E. Derat, Y. Zhang, M. Ménand, S. Roland and M. Sollogoub, *Angew. Chem., Int. Ed.*, 2017, **56**, 10821–10825.
8 S. Roland, J. M. Suarez and M. Sollogoub, *Chem. – Eur. J.*, 2018, **24**, 12464–12473.
9 B. Tang, J. Zhao, J.-F. Xu and X. Zhang, *Chem. – Eur. J.*, 2020, **26**, 15446–15460.
10 C. Zhao, F. D. Toste, K. N. Raymond and R. G. Bergman, *J. Am. Chem. Soc.*, 2014, **136**, 14409–14412.
11 B. Mondal and P. S. Mukherjee, *J. Am. Chem. Soc.*, 2018, **140**, 12592–12601.
12 S. S. Nurttila, W. Brenner, J. Mosquera, K. M. van Vliet, J. R. Nitschke and J. N. H. Reek, *Chem. – Eur. J.*, 2019, **25**, 609–620.
13 J. Guo, Y.-W. Xu, K. Li, L.-M. Xiao, S. Chen, K. Wu, X.-D. Chen, Y.-Z. Fan, J.-M. Liu and C.-Y. Su, *Angew. Chem., Int. Ed.*, 2017, **56**, 3852–3856.
14 H. Takezawa, T. Kanda, H. Nanjo and M. Fujita, *J. Am. Chem. Soc.*, 2019, **141**, 5112–5115.
15 Q. Zhang, L. Catti and K. Tiefenbacher, *Acc. Chem. Res.*, 2018, **51**, 2107–2114.
16 A. Cavarzan, A. Scarso, P. Sgarbossa, G. Strukul and J. N. H. Reek, *J. Am. Chem. Soc.*, 2011, **133**, 2848–2851.
17 J. Kang and J. Rebek, *Nature*, 1997, **385**, 50–52.
18 Y. Yu, J.-M. Yang and J. Rebek, *Chem*, 2020, **6**, 1265–1274.
19 J. L. Bolliger, in *Effects of Nanoconfinement on Catalysis*, ed. R. Poli, Springer International Publishing, Cham, 2017, pp. 17–48, DOI: 10.1007/978-3-319-50207-6_2.
20 K. I. Assaf and W. M. Nau, *Chem. Soc. Rev.*, 2015, **44**, 394–418.
21 S. J. Barrow, S. Kasera, M. J. Rowland, J. del Barrio and O. A. Scherman, *Chem. Rev.*, 2015, **115**, 12320–12406.
22 T.-C. Lee, E. Kalenius, A. I. Lazar, K. I. Assaf, N. Kuhnert, C. H. Grün, J. Jänis, O. A. Scherman and W. M. Nau, *Nat. Chem.*, 2013, **5**, 376–382.
23 X. Qiu, Y. Wang, S. Leopold, S. Lebedkin, U. Schepers, M. M. Kappes, F. Biedermann and S. Bräse, *Small*, 2023, 2307318.
24 S. Angelos, Y.-W. Yang, K. Patel, J. F. Stoddart and J. I. Zink, *Angew. Chem., Int. Ed.*, 2008, **47**, 2222–2226.
25 D. Tuncel, Ö. Özsar, H. B. Tiftik and B. Salih, *Chem. Commun.*, 2007, 1369–1371, DOI: 10.1039/B616764K.
26 T. G. Brevé, M. Filius, C. Araman, M. P. van der Helm, P.-L. Hagedoorn, C. Joo, S. I. van Kasteren and R. Eelkema, *Angew. Chem., Int. Ed.*, 2020, **59**, 9340–9344.
27 Y. Kang, X. Tang, H. Yu, Z. Cai, Z. Huang, D. Wang, J.-F. Xu and X. Zhang, *Chem. Sci.*, 2017, **8**, 8357–8361.
28 X. Tang, Z. Huang, H. Chen, Y. Kang, J.-F. Xu and X. Zhang, *Angew. Chem., Int. Ed.*, 2018, **57**, 8545–8549.
29 D. Li, Z. Feng, Y. Han, C. Chen, Q.-W. Zhang and Y. Tian, *Adv. Sci.*, 2022, **9**, 2104790.
30 N. Zhao, L. Liu, F. Biedermann and O. A. Scherman, *Chem. – Asian J.*, 2010, **5**, 530–537.
31 R. C. Laird, M. A. Sinnwell, N. P. Nguyen, D. C. Swenson, S. V. S. Mariappan and L. R. MacGillivray, *Org. Lett.*, 2015, **17**, 3233–3235.
32 D. Sigwalt, M. Šekutor, L. Cao, P. Y. Zavalij, J. Hostaš, H. Ajani, P. Hobza, K. Mlinarić-Majerski, R. Glaser and L. Isaacs, *J. Am. Chem. Soc.*, 2017, **139**, 3249–3258.
33 H. Wu, Y. Wang, L. O. Jones, W. Liu, B. Song, Y. Cui, K. Cai, L. Zhang, D. Shen, X.-Y. Chen, Y. Jiao, C. L. Stern, X. Li, G. C. Schatz and J. F. Stoddart, *J. Am. Chem. Soc.*, 2020, **142**, 16849–16860.

 This journal is © The Royal Society of Chemistry 2024